

Detecting the non-Gaussian Spectrum of QSO's Ly α Absorption Line Distribution

Jesús Pando^{1,2} and Li-Zhi Fang²

¹ UMR 7550 CNRS, Observatoire de Strasbourg, 67000 Strasbourg, France
pando@wirtz.u-strasbg.fr

² Department of Physics, University of Arizona, Tucson, AZ 85721, USA
fanglz@physics.arizona.edu

Received date / Accepted date

Abstract. We present an analysis of the non-Gaussianity in the distribution of Ly α forest lines in the QSO absorption spectra. Statistical tests performed on this data indicate that there may be large scale structure even though the power spectrum of the Ly α line distribution on large scales is found to be flat. It is apparent that higher (than two) order statistics are crucial in quantifying the clustering behavior of Ly α clouds.

A method of detecting the spectrum of cumulants of the discrete wavelet transform (DWT) coefficients is developed. Because the basis of the DWT is compactly supported, the DWT is not subject to the central limit theorem. Cumulants of any order can be quickly computed and serve as a way of detecting non-Gaussianity.

Using this technique on three independent data sets of Ly α forests, we find that the distribution of Ly α forests does show non-Gaussian behavior on scales from 5 to 10 h⁻¹ Mpc with confidence level larger than 95%. Two data sets available on large scales are found to be non-Gaussian on even larger scales. These techniques are effective in discriminating among models of the Ly α forest formation, which are degenerate at second and lower order statistics.

Key words: cosmology: large-scale structure of Universe – quasars: absorption lines

1. Introduction

Ly α absorption line forests in QSO spectra come from intervening absorbers, or clouds, with neutral hydrogen column densities ranging from about 10¹² to 10¹⁷ cm⁻² at high redshifts. Since the size of the Ly α clouds at high redshift is as large as 100 - 200 h⁻¹ Kpc, and their velocity dispersion is as low as \sim 100 km s⁻¹ (Bechtold et al. 1994, Dinshaw et al. 1995, Fang et al. 1996), it is generally believed that the Ly α forests are due to the absorption of pre-collapsed clouds in the density field of the universe. Ly α clouds are probably fair tracers of the cosmic density field on large scales and therefore,

the clustering behavior of the Ly α clouds should be useful for testing models of structure formation of the universe.

More importantly, unlike other high redshift objects, Ly α forests do not show significant power in their two-point correlation functions. Aside from very small scales $\Delta v \leq 300$ km/s, all results drawn from the two-point correlation function of the Ly α absorption lines have failed to detect clustering (Webb, 1987, Weymann 1993, Hu et al. 1995, Cristiani et al. 1997). The power spectrum of the 1-D spatial distribution of the Ly α absorbers is found to be flat on scales in velocity space of \sim 600 to 30,000 km s⁻¹ (Pando & Fang 1998). This result indicates that the distribution of the Ly α clouds may still be in the linear or quasilinear evolutionary stages on scales larger than a few h⁻¹ Mpc. Indeed, it is found that simulations of popular models using the linear or log-normal approximation fit well with the second order statistical properties of Ly α forests (Bi, Ge & Fang 1995, Bi & Davidson 1997). Therefore, the Ly α clouds may contain information of cosmic clustering in the linear or quasilinear evolutionary stages.

It is known that even though the evolution of the power spectrum during the quasi-linear regime does not significantly differ from the linear regime, the density perturbations on different scales will no longer evolve mutually independently because of the power transfer of perturbations via mode coupling. For popular models, like the cold dark matter model, the mode-mode coupling of the quasi-linear evolution leads to a power transfer from large scales to small ones (Suto & Sasaki 1991). Numerical studies show that the power transfer is already significant on scales of about 50 h⁻¹ Mpc at redshift \sim 2 (Jing et al. 1995). Thus, there should exist non-Gaussianity on scales of a few 10 h⁻¹ Mpc which is the “remnant” of the mode-mode coupling of the quasi-linear evolution.

This theory is supported by works based on methods other than the two-point correlation function. For instance, the distribution of nearest neighbor Ly α line intervals is found to be definitely different from a Poisson process (Duncan, Ostriker, & Bajtlik 1989; Liu and Jones 1990). A study using the Kolmogorov-Smirnov (K-S) statistic, finds that Ly α absorbers show a deviation from a uniform random distribution at the $\sim 3\sigma$ significance level (Fang, 1991). Some observations also

indicate the existence of ~ 10 Mpc void (Dobrzycki & Bechtold 1991), and deviation from uniform distribution on larger scales (Crofts 1987, 1989.) However, this individual structure cannot be used for a statistical analysis. Using a method based on cluster identification, many structures have been systematically identified and formed into an ensemble. It is found that the abundance of the identified “clusters” with respect to the richness are significantly different from a Gaussian process (Pando & Fang 1996, hereafter PF). Recently, we have also found that the Ly α forest line distribution shows significant scale-scale correlations. As a consequence models which predict a Gaussian process for the evolution of the Ly α clouds are ruled out, and the halos hosting the clouds must have gone through a “history” dependent merging process during their formation (Pando et al. 1998.)

In this paper, we will continue to develop the description of the non-Gaussianity of the Ly α line distribution. The emphasis of this paper will be to detect the non-Gaussian spectrum, and to show its ability to discriminate among models of Ly α cloud formation which are degenerate at second order.

In §2, we will describe the observed and simulated samples of Ly α forests, and the problems related to their large scale structure detection. In §3, the DWT technique of non-Gaussian spectrum detection will be discussed. The results of this analysis for real and simulated samples are discussed in §4. We will show that the distributions of Ly α forest lines are significantly different from Gaussian distributions. Additionally, we show that the non-Gaussian spectrum is a powerful tool for distinguishing between models.

2. Ly α samples and problems

In PF, we looked at two popular data sets of Ly α forests. The first compiled by Lu, Wolfe and Turnshek (1991, hereafter LWT) contains ~ 950 lines from the spectra of 38 QSO that exhibit neither broad absorption lines nor metal line systems. The second set is from Bechtold (1994, hereafter JB), which contains ~ 2800 lines from 78 QSO's spectra, in which 34 high red-shift QSOs were observed at moderate resolution. In this paper, we augment those data sets with two observations using the Keck telescope: 1) Hu et al. (1995, hereafter HKCSR) observed 4 QSO's with a total of 1056 lines and column density in the range $N_{HI} \geq 2 \times 10^{12} \text{ cm}^{-2}$ at extremely high S/N; 2) Kirkman and Tyler (1997, hereafter KT) obtained the highest quality spectra published to date from QSO HS 1946+7658 with 466 Ly α forest lines. A typical sample is shown in Figure 1, which is a 1-D histogram of the spatial distribution of Ly α absorption lines of QSO-0142.

It is well known that the number density of the Ly α absorption lines increases with red-shift. The number density of lines with rest equivalent width W greater than a threshold W_{th} can approximately be described as

$$\frac{dN}{dz} = \left(\frac{dN}{dz} \right)_0 (1+z)^\gamma, \quad (1)$$

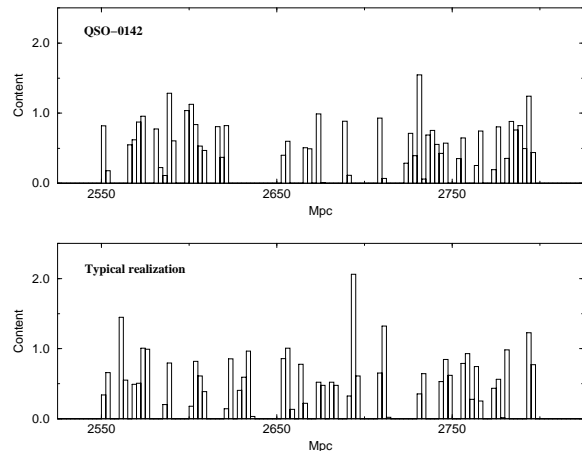


Fig. 1. The Ly α forest line distribution of sample Q0142 and a typical realization of its randomization.

where $(dN/dz)_0$ is the number density extrapolated to zero red-shift, and γ the index of evolution. LWT finds that $(dN/dz)_0 \simeq 3$ and $\gamma = 2.75 \pm 0.29$ for lines with $W \geq W_{th} = 0.36 \text{ \AA}$. KT finds $\gamma = 2.6$ while JB finds that $\gamma = 1.89 \pm 0.28$ for $W_{th} \geq 0.32 \text{ \AA}$ and $\gamma = 1.32 \pm 0.24$ for $W_{th} \geq 0.16 \text{ \AA}$.

Like other Ly α forest data, these data sets have failed to reveal structures in their distribution on scales $\Delta v \geq 300 \text{ km/s}$ when subjected to a two point correlation analysis (Hu et al. 1995.) Using the discrete wavelet transform spectrum estimator, the Fourier power spectrum of the 1-dimensional (1-D) spatial distribution of these data is found to be almost flat on scales from 2 to about $100 \text{ h}^{-1} \text{ Mpc}$ (Pando & Fang 1998). For comparison, Figure 1 also shows a randomized sample which is produced by a random shifting of the lines of QSO-0142. Obviously, one cannot simply distinguish the real sample and its random counterpart by inspection. In fact, when analyzed by second order statistics, the real data are still indistinguishable from randomized samples.

These results indicate that 2nd order statistical techniques, i.e. the two-point correlation function and the power spectrum, are not even qualitatively sufficient to describe the clustering features of these samples. Higher order measures are not a correction to lower order descriptions, but crucial in describing the Ly α forest traced matter field.

This conclusion is strengthened by studying simulated samples. Typically, simulated density fields for pre-collapsed clouds are generated as perturbations with a linear or linear log-normal spectrum given by models such as the cold dark matter model (SCDM), the cold plus hot dark matter model (CHDM), and the low density flat cold dark matter model (LCDM). The baryonic matter distribution is then produced by assuming that the baryonic matter traces the dark matter distribution on scales larger than the Jeans length of the baryonic gas, but is smooth over structures on scales less than the Jeans length. The simulated Ly α absorption spectrum can be calculated as the absorption of neutral hydrogen in the baryonic gas. The effects of the observational instrumental point-spread-function, along with

Poisson and background noises can also be simulated properly (Bi, Ge & Fang 1995, hereafter BGF; Bi & Davidson 1997).

Within a reasonable set of parameters, the simulated samples are found to fit with observational measurements such as the number density of Ly α clouds, the distribution of equivalent widths, the red-shift-dependence of the width distributions and clustering. Regardless the details of the simulation, these samples should contain structures because the effects of gravitational collapse have been considered, and baryonic matter does not distribute uniformly random, but traces the structure of dark matter. However, as is the case with observations, the simulated samples show no power in their two-point correlations (see Figure.11 of BGF), and their 1-D spectra are rather flat on scales less than 100 h $^{-1}$ Mpc. These results clearly show that higher order measures are necessary in describing the statistical features of the 1-D distributions of the Ly α clouds.

3. Higher Order Statistics via the Wavelet Coefficients

3.1. DWT decomposition and 2nd Order Statistics

It is generally believed that the cosmic mass (or number) density distribution $\rho(x)$ can be mathematically treated as a homogeneous random field. It is often more convenient to express $\rho(x)$ in terms of its Fourier transform, $\rho(k)$, which is the Fourier coefficient of $\rho(x)$.

One reason for expressing the density distribution in terms of its Fourier transform is that for Gaussian random fields all the statistical features of $\rho(x)$ can be completely described by the amplitude of the Fourier coefficients. In this case, the phase of $\rho(k)$ is not important and the power spectrum of the perturbations, $|\rho(k)|^2$, or equivalently, the two-point correlation function, are all that is necessary to describe the statistical behavior of the density distribution. However, if the field $\rho(x)$ is non-Gaussian, then in order to have a full statistical description of the field the phases of the Fourier coefficients $\rho(k)$ are essential.

As is well known, it is difficult, even practically impossible, to find information about the phases of the Fourier coefficient as soon as there is some computational noise. The lack of information about the phases makes the $\rho(k)$ description incomplete: we might know the scales k of the structures, but nothing about the positions of the considered structures. A possible way of simultaneously describing the scale and position of structures is provided by the discrete wavelet transform (DWT) (Daubechies 1992, Meyer 1993.) The DWT analysis has successfully been applied to the problems of turbulence (Yamada & Ohkitani 1991; Farge 1992) and high energy physics (Huang et al. 1996.) Our previous studies also show that the DWT analysis is useful for large scale structure study (Pando & Fang 1996, Fang & Pando 1997, 1998; Pando et al. 1998, Fang, Deng & Xia, 1998, Xu, Fang & Wu, 1998.)

Let's consider a 1-D mass density contrast $\delta(x) = [\rho(x) - \bar{\rho}]/\bar{\rho}$, which covers a spatial range $0 \leq x \leq L$. The expansion of the field $\rho(x)$ in terms of the DWT basis is given by

$$\delta(x) = \sum_{j=0}^{\infty} \sum_{l=0}^{2^j-1} \tilde{\delta}_{j,l} \psi_{j,l}(x) \quad (2)$$

where $\psi_{j,l}(x)$, $j = 0, 1, \dots$, $l = 0 \dots 2^j - 1$ are the basis of the DWT. The DWT basis are orthogonal and complete. The wavelet function coefficient (WFC), $\tilde{\delta}_{j,l}$, is computed by

$$\tilde{\delta}_{j,l} = \int \delta(x) \psi_{j,l}(x) dx. \quad (3)$$

The wavelet transform basis functions $\psi_{j,l}(x)$ are generated from the basic wavelet $\psi(x/L)$ by a dilation, 2^j , and a translation l , i.e.

$$\psi_{j,l}(x) = \left(\frac{2^j}{L}\right)^{1/2} \psi(2^j x/L - l). \quad (4)$$

The basic wavelet ψ is designed to be continuous, admissible and localized. Unlike the Fourier basis $\exp(-i2\pi n x/L)$, which are non-local in physical space, the wavelet basis $\psi_{j,l}(x)$ are localized in both physical space and Fourier (scale) space. In physical space, $\psi_{j,l}(x)$ is centered at position $lL/2^j$, and in Fourier space, it is centered at wavenumber $2\pi \times 2^j/L$. Therefore, the WFCs, $\tilde{\delta}_{j,l}$, have two subscripts j and l , which describe, respectively, the scale and position of the density perturbations.

A clearer picture of how the transforms work can be seen in the phase space (x, k) . A complete, orthogonal basis set resolves the whole phase space into "elements" of size Δx and Δk . Each mode corresponds to elements in the phase space. For the Fourier transform, this corresponds to elements of size $\Delta k = 0$ and $\Delta x = \infty$. For the wavelet transform, both Δk and Δx are finite, and the corresponding area of the element is as small as $\Delta x \Delta k = 2\pi$. That is, the DWT is able to resolve an arbitrary function simultaneously in terms of x and k up to the limit of the uncertainty principle. The DWT decomposes the density fluctuation field $\delta(x)$ into domains j, l in phase space, and for each mode, the corresponding area in the phase space is as small as that allowed by the uncertainty principle.

The WFC $\tilde{\delta}_{j,l}$ and its intensity $|\tilde{\delta}_{j,l}|^2$ describe, respectively, the fluctuation of the density and its power on scale $L/2^j$ at position $lL/2^j$. As with the Fourier basis, Parseval's theorem holds for the DWT basis. It is (Fang & Pando 1997, Pando & Fang, 1998)

$$\frac{1}{L} \int_0^L |\delta(x)|^2 dx = \sum_{j=0}^{\infty} \sum_{l=0}^{2^j-1} |\tilde{\delta}_{j,l}|^2. \quad (5)$$

It is possible to define the power spectrum of the density perturbation on scale j by the variance of the WFCs as

$$P_j = \sum_{l=0}^{2^j-1} (\tilde{\delta}_{j,l} - \overline{\tilde{\delta}_{j,l}})^2, \quad (6)$$

where

$$\overline{\tilde{\delta}_{j,l}} \equiv \frac{1}{2^j} \sum_{l=0}^{2^j-1} \tilde{\delta}_{j,l}. \quad (7)$$

It has been shown that the DWT power spectrum eq.(6) can be converted to the Fourier power spectrum, i.e. in terms of second order statistical description the DWT and Fourier transform are equivalent.

3.2. One-point distribution of WFCs and non-Gaussianity

The cosmic density field is usually assumed to be ergodic: the average over an ensemble is equal to the spatial average taken over one realization. This is the so-called ‘‘fair sample hypothesis’’ (Peebles 1980). A homogeneous Gaussian field with continuous spectrum is certainly ergodic (Adler 1981). In some non-Gaussian cases, such as homogeneous and isotropic turbulence (Vanmarke, 1983), ergodicity also approximately holds. Roughly, the ergodic hypothesis is reasonable if spatial correlations are decreasing sufficiently rapidly with increasing separation. In this case, the volumes separated by large distances are approximately statistically independent, and can be treated as independent realizations. Note that the $\psi_{j,l}(x)$ are orthogonal with respect to the position index l , and therefore, for an ergodic field, the 2^j WFCs, $\tilde{\delta}_{j,l}$, $l = 0, 1, \dots, 2^j - 1$, at a given j should be statistically independent. Thus the WFCs $\tilde{\delta}_{j,l}$ at fixed j and different l can be treated as independent measures of the density fluctuation field. The 2^j WFCs, $\tilde{\delta}_{j,l}$, from one realization of $\delta(x)$ can be employed as a statistical ensemble. In this way, when the fair sample hypothesis holds, an average of the ensemble can be well estimated by averaging over l , i.e. $\langle \tilde{\delta}_{j,l} \rangle \simeq (1/2^j) \sum_{l=0}^{2^j-1} \tilde{\delta}_{j,l}$, where $\langle \dots \rangle$ denotes the ensemble average.

Consequently, the distribution of the $\tilde{\delta}_{j,l}$ is actually the one-point distribution of the WFCs at a given scale j . The non-Gaussianity of the density field $\delta(x)$ can directly be measured by the deviation of the one-point distribution from a Gaussian distribution. For this purpose, we can calculate the cumulant moments defined by (Carruthers 1991; Carruthers, Eggers & Sarcevic 1991)

$$I_j^2 = M_j^2, \quad (8)$$

$$I_j^3 = M_j^3, \quad (9)$$

$$I_j^4 = M_j^4 - 3M_j^2 M_j^2, \quad (10)$$

$$I_j^5 = M_j^5 - 10M_j^3 M_j^2, \quad (11)$$

where

$$M_j^n \equiv \frac{1}{2^j} \sum_{l=0}^{2^j-1} (\tilde{\delta}_{j,l} - \overline{\tilde{\delta}_{j,l}})^n. \quad (12)$$

From eqs.(6), (7) and (8), one sees that the second order cumulant moment is the DWT power spectrum on the scale j , i.e.

$$I_j^2 = \frac{1}{2^j} P_j. \quad (13)$$

For Gaussian fields all the cumulant moments higher than order 2 are zero. Thus one can measure the non-Gaussianity of the density field $\delta(x)$ by I_j^n with $n > 2$. Analogous to I_j^2 being called the DWT power spectrum, we will call I_j^n the DWT spectrum of n -th cumulant. The cumulant measures I_j^3 and I_j^4 are related to the better known skewness and kurtosis, respectively. Thus, the non-Gaussianity of $\delta(x)$ can be detected by the DWT skewness and kurtosis spectra defined as

$$S_j \equiv \frac{1}{(I_j^2)^{3/2}} I_j^3, \quad (14)$$

$$K_j \equiv \frac{1}{(I_j^2)^2} I_j^4. \quad (15)$$

S_j and K_j are basic statistical measures employed in this paper.

For comparison, the definitions of the ‘‘standard’’ skewness S and kurtosis K for a 1-D distribution $\delta(x)$ covering on N bins are given as follows

$$S \equiv \frac{1}{N\sigma^3} \sum_{i=1}^N (\delta(x_i) - \overline{\delta(x_i)})^3, \quad (16)$$

and

$$K \equiv \frac{1}{N\sigma^4} \sum_{i=1}^N [(\delta(x_i) - \overline{\delta(x_i)})^4] - 3, \quad (17)$$

where the variance σ^2 is given by

$$\sigma^2 \equiv \frac{1}{N-1} \sum_{i=1}^N (\delta(x_i) - \overline{\delta(x_i)})^2. \quad (18)$$

Obviously, no scale information is given by S and K .

3.3. Central limit theorem and the DWT analysis

It is well known that not all one-point distributions can detect non-Gaussianities. This is due to the constraints imposed by the central limit theorem. For instance, if the universe consists of a large number of dense clumps with a non-Gaussian probability distribution function (PDF), the one-point distributions of the real and imaginary components of each individual Fourier mode are still Gaussian due to the central limit theorem (Ivanov & Leonenko 1989). Further, even when the non-Gaussian clumps are correlated the central limit theorem still holds if the two-point correlation function of the clumps approaches zero sufficiently fast (Fan & Bardeen 1995). For these reasons, the one-point distribution function of Fourier modes is not sensitive enough to detect deviations from Gaussian behavior. Even for samples with strong non-linear evolution, the one point distribution function of Fourier modes is found to be consistent with a Gaussian distribution (Suginohara & Suto 1991). It should be pointed out that the inefficiency of the Fourier mode one-point distribution in detecting non-Gaussianity is not because Fourier transform loses information about the distribution $f(x)$. The Fourier coefficients contain all the information

on non-Gaussianity, but the information is mainly contained in the phases of the Fourier coefficients. As mentioned in §3.1, it is very difficult to detect the distribution of the phases of Fourier coefficients.

On the other hand, the wavelet coefficients are not subject to the central limit theorem. In this respect, the DWT analysis is similar to the count in cell (CIC) method (Hamilton 1985; Alimi, Blanchard & Schaeffer 1990; Gaztañaga & Yokoyama 1993; Bouchet et al. 1993; Kofman et al. 1994; Gaztañaga & Frieman 1994). The CIC is not subject to the central limit theorem as it based on spatially localized window functions (Adler 1981). The DWT's basis are also localized. If the scale of a clump in the universe is d , eq.(3) shows that the WFCs, $\tilde{\delta}_{j,l}$, with $j = \log_2(L/d)$, is determined only by the density field in a range containing no more than one clump. That is, for scale j the wavelet coefficients are not given by a superposition of a large number of clumps, but are determined by at most one of them. Therefore, it avoids the constraints imposed by the central limit theorem.

This point can also be shown from the orthonormal basis being used for the expansion of the distribution $\delta(x)$. A basic condition of the central limit theorem is that the modulus of the basis be less than C/\sqrt{L} , where C is a constant (Ivanov & Leonenko 1989). Obviously, all Fourier-related orthonormal basis satisfy this condition because $(1/\sqrt{L})|\sin kx| < C/\sqrt{L}$ and $(1/\sqrt{L})|\cos kx| < C/\sqrt{L}$, where C is independent of coordinates in both physical space x and scale space k . On the other hand, the normalized wavelets functions have [eq.(4)]

$$|\psi_{j,l}(x)| \sim \left(\frac{2^j}{L}\right)^{1/2} O(1). \quad (19)$$

Because the magnitude of the basic wavelet $\psi(x)$ is of order 1. The condition $|\psi_{j,l}(x)| < C/\sqrt{L}$ will no longer hold for a constant C independent of scale variable j . Hence, the one-point-distribution of wavelet coefficients on scale j should be a good estimator for the PDF of a distribution.

4. Skewness and kurtosis spectra of Ly α forests

4.1. Data preparation

The observational QSO Ly α forests data have a complex geometry. By this we mean that different forests cover different spatial ranges, and no one of the forests distributes on the entire range (D_{min}, D_{max}). At the very least, a complicated weighting scheme is needed in order to form an ensemble. The DWT provides a way around this problem. Because wavelets are localized, the wavelet coefficients are only determined by the local distribution. If a forest sample lies in range (D_1, D_2), one can extend it to (D_{min}, D_{max}) by adding zeros to the data in ranges (D_{min}, D_1) and (D_2, D_{max}). The wavelet coefficients in the interval (D_1, D_2) will not be affected by the addition of zero in (D_{min}, D_1) and (D_2, D_{max}). Any statistics can then be computed by the ensemble of wavelet coefficients, $\tilde{\delta}_{j,l}$, by simply dropping all wavelet coefficients with l in the added zero ranges.

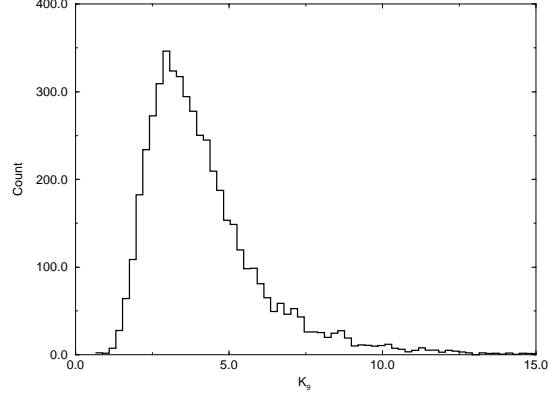


Fig. 2. Frequency distributions of K_9 from 5000 random samples. It can be clearly seen that this distribution is non-Gaussian.

More precisely, the effect of zero padding on the wavelet coefficients is described by the so-called “influence cone” which consists of the spatial support of all dilated wavelet functions. For instance, if $\psi_{j,l}(x)$ is localized in the space interval Δx for $j = 0$, the influence cone centered at x_0 is given by $x \in [x_0 - (\Delta x/2^{j+1}), x_0 + (\Delta x/2^{j+1})]$ (Farge 1992). Wavelet coefficients corresponding to positions outside $(\Delta x/2^{j+1})$ will not corrupt information within the influence cone.

The LWT and JB samples cover a red-shift range of 1.7 to 4.1, i.e. the spatial range in comoving distance is from about $D_{min}=2,300 h^{-1}\text{Mpc}$ to $D_{max}=3,300 h^{-1}\text{Mpc}$, if $q_0 = 1/2$ and $h= H_0/100 \text{ km s}^{-1} \text{ Mpc}^{-1}$. To eliminate the proximity effect, all lines with $z \geq z_{em} - 0.15$ are deleted from our samples. These two samples are extended to (D_{min}, D_{max}) as described above, and binned into 512 bins with comoving size $\sim 2.5 h^{-1} \text{ Mpc}$, which is about the scale where the effect of line blending occurs. If a line is not located at the center of a bin, it is separated into the two neighboring bins, weighted according to the distance to each of the centers.

The HKCSR and KT samples (HKCSR+KT), can be treated the same way. Since HKCSR and KT cover a smaller red-shift range from about 2.4 to 3.1, the forests of HKCSR+KT are extended to 128 bins of comoving size $\sim 2.5 h^{-1} \text{ Mpc}$. Thus it is possible to compare all 3 sets for scales down to $j = 6$.

4.2. Skewness and kurtosis spectra of real data

As opposed to $\delta(x)$ discussed in §3, real data provide only histograms of Ly α line distributions, i.e. the data are not a continuous function of x , but a point process in x space. In this case, the WFCs $\tilde{\delta}_{j,l}$ will not be calculated by an integral like eq.(3), but by the wavelet transformation matrix (Press et al. 1992.)

It is well known that point processes generally are non-Gaussian. For instance, if the Ly α clouds do not distribute structurally, then $\delta(x)$ should be a 1-D Poisson process. How-

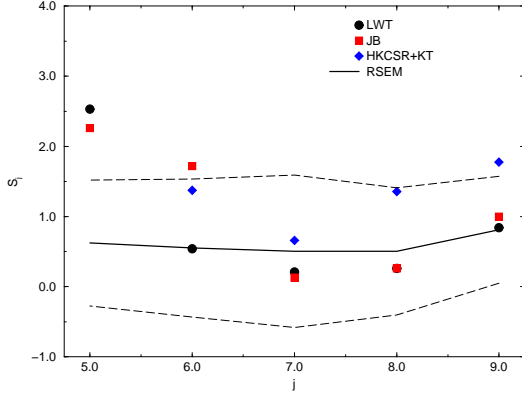


Fig. 3. Skewness spectrum for LWT ($W > 0.36\text{\AA}$), JB ($W > 0.32\text{\AA}$) and HKCSR+KT samples. The red-shift evolution model (RSEM) given by eq. (1), and the 95% confidence limits are also shown. The physical scale is related to j by $2.5 \times 2^{10-j} \text{ h}^{-1} \text{ Mpc}$.

ever, Poisson processes are non-Gaussian. Obviously, this non-Gaussianity is not what we are seeking to measure because it is not the result of non-linear evolution or physical processes related to structure formation. Therefore, we should carefully distinguish the clustering related non-Gaussianity with that from sampling and binning. For this purpose, we generate 5000 random realizations in which the mean number density follows eq.(1). Each realization is treated in the same way as the real data sets. From these random samples we can produce frequency distributions for each statistic, say K_9 (Figure 3). These frequency distributions are fair estimators of the underlying probability distribution. It can clearly be seen from Figure 2 that the random data are non-Gaussian.

Using these frequency distributions, the confidence levels for the mean values of the random data can be estimated. These are then to be compared with the real data.

The skewness and kurtosis spectra of the LWT ($W > 0.36 \text{\AA}$), JB ($W > 0.32 \text{\AA}$) and HKCSR+KT ($b > 78 \text{ km s}^{-1}$) data are shown in Figures 3 and 4, respectively. The skewness and kurtosis spectra of random data and the 95% confidence levels are also shown in these figures. Figures 3 and 4 show that the skewness and the kurtosis spectra of the LWT ($W > 0.36\text{\AA}$) and JB ($W > 0.32\text{\AA}$) are almost the same. The kurtosis spectra are $> 95\%$, significantly different from the random samples on all scales, and, on scales $j = 5$, the skewness spectra are also $> 95\%$ and significantly different from the random samples. The Keck data, i.e. HKCSR+KT, have qualitatively the same non-Gaussian behavior, especially at K_8 and K_9 , where the HKCSR+KT data are the same as that of LWT and JB. The HKCSR+KT gives lower values for K_6 and K_7 than the LWT and JB, while it gives higher S_8 and S_9 than LWT and JB. With the current data it is not possible to determine whether these differences are due to the higher resolution of the HKCSR+KT data. It is important to realize that these observational data sets

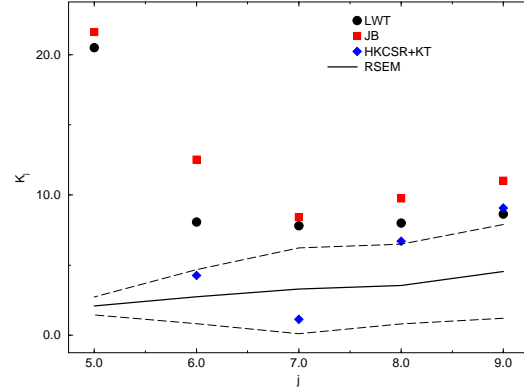


Fig. 4. Kurtosis spectrum for LWT ($W > 0.36\text{\AA}$), JB ($W > 0.32\text{\AA}$) and HKCSR+KT samples. The red-shift evolution model (RSEM) given by eq. (1), and the 95% confidence limits are also shown.

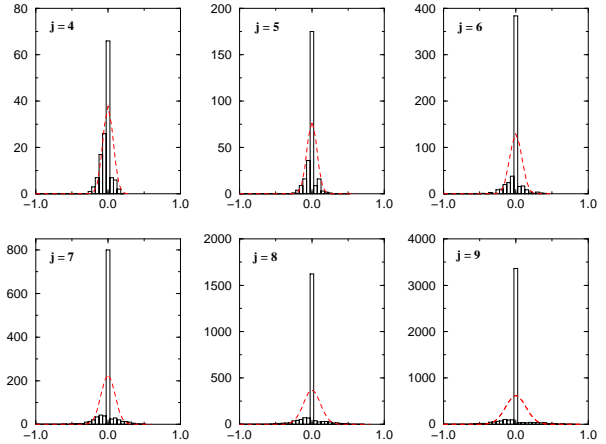


Fig. 5. Histogram of one-point distribution of wavelet coefficients for JB ($W > 0.32\text{\AA}$). At each scale j , the Gaussian distribution (dashed line) has the same variance and normalization as the wavelet coefficient distribution.

were compiled by different groups, on different instruments, and as much as 6 years apart. These data sets are very independent and makes more convincing the case for the existence of the non-Gaussianity at least on scales of 5 - 10 $\text{h}^{-1} \text{ Mpc}$, and confirms that the features shown in the non-Gaussian spectrum are intrinsic features of the density field traced by Ly α forests.

We can directly describe the non-Gaussianity by the one-point distributions of the WFCs. Figure 5 plots the one-point distributions of $\tilde{\delta}_{j,l}$ for the JB sample with $> 0.32\text{\AA}$. For each scale j , the corresponding Gaussian distribution is plotted such that it has the same normalization and variance as the one-point distribution. This figure clearly shows that all the distributions on scales $j > 4$ (or less than about $80 \text{ h}^{-1} \text{ Mpc}$) are significantly non-Gaussian. These distributions are also asymmetric, with fewer positive wavelet coefficients.

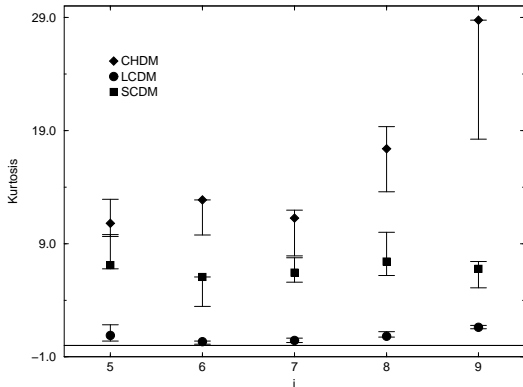


Fig. 6. Kurtosis spectrum of BGF samples in the SCDM, LCDM, and CHDM models with $W \geq 0.32\text{\AA}$.

This asymmetry is at least partially due to the red-shift-dependence of the $\text{Ly}\alpha$ clouds. The wavelet coefficient $\tilde{\delta}_{j-1,l}$ is mainly determined by the difference of (positive) densities at $\{j, 2l\}$ and $\{j, 2l + 1\}$ (PF). For a clump in red-shift space, the density change on the lower red-shift or lower l side contributes negative wavelet coefficients, while the higher red-shift side gives positive wavelet coefficients. If as shown in PF, the number of $\text{Ly}\alpha$ clumps decreases with increasing red-shift, the change in clustering amplitudes (wavelet coefficients) on the higher red-shift side (positive wavelet coefficients) should be less than the lower side (negative wavelet coefficients). That is, the number of positive wavelet coefficients will be less than negative wavelet coefficients. This is consistent with a small, but positive skewness.

4.3. Removing degeneracy by the non-Gaussian spectrum

We have shown that cluster identification by a wavelet decomposition is a useful tool for discriminating among models of $\text{Ly}\alpha$ clouds (PF). The spectrum of non-Gaussianity can play the same role. Namely, S_j and K_j are effective measures for removing the degeneracy that exists at second order among models.

As an example, we examined the BGF simulated $\text{Ly}\alpha$ forest samples. This simulation shows that two models, SCDM and LCDM, are degenerate if only the first (number density) and second (variance, or power spectrum) order statistics are considered. That is, both SCDM and LCDM give about the same predictions for the following features of the $\text{Ly}\alpha$ forests: a.) the number density of $\text{Ly}\alpha$ lines and its dependencies on red-shift and equivalent width; b.) the distribution of equivalent widths and its red-shift dependence; c.) the two-point correlation function.

This degeneracy can be removed by the non-Gaussian spectrum. Figure 6 plots the kurtosis spectra for the LCDM, SCDM, and CHDM models, in which the $\text{Ly}\alpha$ lines are chosen with

width $W > 0.32\text{\AA}$. The error bars in Figure 6 are given by the distribution of 20 realizations for each model.

Figure 6 shows that even though the BGF simulation is based on the linear power spectrum of the density perturbations, the $\text{Ly}\alpha$ distribution is non-Gaussian. This is because the selection of peaks from the density field is a non-Gaussian process. More important, Figure 7 clearly shows the significant difference among the three models. With 95% confidence, the K_j amplitudes of all three models are different on all scales. The K_j of the SCDM model is significantly larger than zero for all scales j . Yet, the LCDM model gives much lower K_j for all scales j . The non-Gaussian spectrum provides an extremely effective method for removing the degeneracy among models.

5. Discussion and conclusions

The DWT skewness and kurtosis spectra of real and simulated samples of $\text{Ly}\alpha$ forests has been calculated. Deviations from a Gaussian state in these samples are detected for all data on scales of 5 to $10 h^{-1}$ Mpc with confidence level larger than 95%. For the two sets which are available on large scales, the non-Gaussianity is significant even on scales as large as about $80 h^{-1}$ Mpc. The scale-dependence (or spectrum) for a higher order DWT cumulant is especially effective in distinguishing the real samples from random data, and in discriminating among models.

It is possible for non-Gaussianity to result from systematic errors hiding in the original data reduction. For instance, discrete sampling or binning of a continuous distribution into a histogram with bin size ΔD leads to non-Gaussianity at least on scale ΔD . Many selection effects actually are some kind of sampling, and therefore, they will also give rise to non-Gaussianity. All these non-Gaussianities are “spurious”.

Fortunately, in most cases these spurious non-Gaussian signals are significant only at one special scale. For a Poisson process, it is the scale of the mean distance of nearest neighbor clouds. For binning, it is ΔD . On scales larger than ΔD , the spurious non-Gaussianities will decay out. That is, the scale-dependent behavior of sampling and binning is useful in recognizing spurious non-Gaussianity. In the case of the $\text{Ly}\alpha$ forests, the mean nearest neighbor distance along with the binning scale ΔD are much less than the scales of the detected non-Gaussianities, and therefore, the detected non-Gaussianities are inherent to the distributions. There is also evidence for intrinsic scales in the $\text{Ly}\alpha$ spectra of magnitude $\sim 25 h^{-1}$ Mpc (Rauch 1998). However this contamination can be reduced by studying K_j and S_j on scales different from $25 h^{-1}$ Mpc.

Nevertheless, high-resolution samples which can cover the spatial range as large as $80 h^{-1}$ Mpc are needed before a final determination can be made. Recently a scale-scale correlation analysis also shows a non-Gaussianity in the $\text{Ly}\alpha$ line distribution on such large scales (Pando et al. 1998). It seems to support our conclusion that cosmic matter underwent a non-Gaussian process on quite large scales at quite early times.

Last but not least, the numerical work of calculating DWT higher order moment spectrum is not any more difficult than

calculating the second order moments. Generally, the calculation of third and higher order correlation functions of large scale structure samples is very strenuous work. But the numerical work involved in calculating the DWT is about the same as the FFT, and can even be faster. The FFT requires $\sim N \log N$ calculations, while the DWT, using a "pyramid" scheme, requires only order N calculations (Press et al. 1992).

This method can easily be generalized to 2- and 3- dimensions. The kurtosis and skewness spectrum opens a new window for looking at the statistical features of large scale structures. It is an important and necessary addition to the existing methods of describing the clustering and correlation of the cosmic density field, and for discriminating among models of structure formation.

Acknowledgements. Both authors wish to acknowledge the debt owed to the late Professor P. Carruthers who initiated the DWT study in our group. He will be sorely missed by us both. We also thank to Drs. H.G. Bi and P.Lipa for insightful conversations.

References

- Adler, R.J. 1981, *The Geometry of Random Field*, (New York, Wiley)
- Alimi, J.M., Blanchard, A. & Schaeffer, R. 1990, ApJ, 402, 38
- Bouchet, F., Strauss, M.A., Davis, M., Fisher, K.B., Yahil, A. & Huchra, J.P. 1993, ApJ, 417, 36
- Bechtold, J. 1994, ApJS, 91, 1.
- Bechtold, J., Crofts, P.S., Duncan, R.C. & Fang, Y. 1994, ApJ, 437, L83
- Bi, H.G & Davidson, A. F., 1997, ApJ, 479, 523.
- Bi, H.G., Ge, J. & Fang, L.Z. 1995, ApJ, 452, 90, (BGF)
- Carruthers, P. 1991, ApJ, 380, 24
- Carruthers, P., Eggers, H.C. & Sarcevic, I. 1991, Phys. Rev. C44, 1623
- Cristiani, S., D'Odorico, S., D'Odorico, V., Fontana, A., Giallongo, E., Saveglio, S., 1997, MNRAS, 285, 209
- Crofts A.P.S. 1987, MNRAS, 228, P41
- Crofts A.P.S. 1989, ApJ, 336, 550
- Dobrzycki, A., Bechtold, J. 1991, ApJ, 377, L69
- Daubechies, I., 1992, *Ten Lectures on Wavelets*, SIAM
- Dinshaw, N., Foltz, C.B., Impey, C.D., Weymann, R. & Morris, S.L., 1995, Nature, 373, 223
- Duncan, R.C., Ostriker, J.P. & Bajtlik, S. 1989, ApJ, 345, 39, see also Bajtlik, S. 1994, in *QSO Absorption Lines*, ed. Meylan, G., Springer, New York
- Fan, Z.H. & Bardeen, J.M. 1995, Phys. Rev. D51, 6714
- Fang, L.Z. 1991, A&A, 244, 1
- Fang, L.Z. and Pando, J. 1997, in *The 5th Current Topics of Astrofundamental Physics*, eds. N.Sanchez and A.Zichichi, World Scientific, Singapore.
- Fang, L.Z., Deng, Z.G. & Xia, X.Y., 1998, ApJ, in press
- Fang, Y.H., Duncan, R.C., Crofts, A.P.S. & Bechtold, J. 1996, ApJ, 462, 77
- Farge, M., 1992, Ann. Rev. Fluid Mech., 24, 395
- Gaztañaga, E. & Frieman, J. 1994, ApJ, 437, L13
- Gaztañaga, E. & Yokoyama, J. 1993, ApJ, 403, 4
- Jing, Y.P., Mo, H.J., Börner, G. & Fang, L. Z. 1995, MNRAS, 276, 417
- Hamilton, A.J.S. 1985, ApJ, 292, L35
- Hu, E.M., Kim, T.S., Cowie, L.L., Songaila, A & Rauch, M. 1995, A.J. 110, 1526 (HKCSR)
- Huang, Z. Sarcevic, I., Thews, R. & Wang, X.N. 1996, Phys. Rev. D. 54, 750
- Ivanov, A.V. & Leonenko, N.N. 1989, *Statistical Analysis of Random Field*, Klumer Academic Pub.
- Kirkman, D. & Tytler, D. 1997, ApJ, 484, 672 (KT)
- Kofman, L., Bertschinger, E., Gelb, J.M., Nusser, A. & Dekel, A. 1994, ApJ, 420, 44
- Liu X.D., Jones B.J.T. 1990, MNRAS, 242, 678
- Lu, L., Wolfe, A.M., & Turnshek, D.A. 1991, ApJ, 367, 19 (LWT)
- Meyer, Y. 1993, *Wavelets: Algorithms and Applications*, SIAM
- Pando, J. & Fang, L.Z. 1996, ApJ, 459, 1 (PF)
- Pando, J. & Fang, L.Z. 1998, Phys. Rev. E57, 3593
- Pando, J., Greiner, M., Lipa, P. & Fang, L.Z. 1998, ApJ, 496, 9
- Peebles, P.J.E. 1980, *The Large Scale Structure of the Universe*, Princeton Univ. Press
- Press, W.H., Flannery, B.P., Teukolsky, S.A. & Vetterling, W.T., 1992, *Numerical Recipes*, Cambridge
- Rauch, M., astro-ph/9806286.
- Suginohara, T. & Suto, Y. 1991, ApJ, 371, 470
- Suto, Y. & Sasaki, M. 1991, Phys. Rev. Lett. 66, 264
- Vanmarke, E.H. 1983, *Random Field*, MIT
- Webb, J.K. 1987, in *Observational Cosmology* eds. A. Hewitt., G. Burbidge, & L.Z. Fang (D. Reidel Pub. Co.)
- Weymann, R.J. 1993, *The Environment and Evolution of Galaxies*, ed. Shull, J.M. & Thronson, H.A. Jr.
- Xu, W., Fang, L.Z. & Wu, X.P. 1998, ApJ, in press
- Yamada, M. & Ohkitani, K. 1991, Prog. Theor. Phys., 86, 799